Editors' Suggestion

Anisotropic Nonlocal Damping in Ferromagnet/α-GeTe Bilayers Enabled by Splitting Energy Bands

Xu Yang,[1,3,5] Liang Qiu,[2] Yan Li,[1,*] Hao-Pu Xue,[1,3] Jia-Nan Liu,[1,3] Rui Sun,[1,3] Qing-Lin Yang,[1,3] Xue-Song Gai,[1,3] Yan-Sheng Wei,[1,3] Andrew H. Comstock,[4] Dali Sun,[4] Xiang-Qun Zhang,[1] Wei He,[1] Yusheng Hou,[2,†] and Zhao-Hua Cheng[1,3,5,‡]

[1]*Beijing National Laboratory for Condensed Matter Physics, Institute of Physics, Chinese Academy of Sciences, Beijing 100190, China*
[2]*Guangdong Provincial Key Laboratory of Magnetoelectric Physics and Devices, Center for Neutron Science and Technology, School of Physics, Sun Yat-Sen University, Guangzhou 510275, China*
[3]*School of Physical Sciences, University of Chinese Academy of Sciences, Beijing 100049, China*
[4]*Department of Physics and Organic and Carbon Electronics Laboratory (ORCEL), North Carolina State University, Raleigh, North Carolina 27695, USA*
[5]*Songshan Lake Materials Laboratory, Dongguan, Guangdong 523808, China*

(Received 8 July 2022; revised 20 July 2023; accepted 6 October 2023; published 3 November 2023)

The understanding and manipulation of anisotropic Gilbert damping is crucial for both fundamental research and versatile engineering and optimization. Although several works on anisotropic damping have been reported, no direct relationship between the band structure and anisotropic damping was established. Here, we observed an anisotropic damping in Fe/GeTe manipulated by the symmetric band structures of GeTe via angle-resolved photoemission spectroscopy. Moreover, the anisotropic damping can be modified by the symmetry of band structures. Our Letter provides insightful understandings of the anisotropic Gilbert damping in ferromagnets interfaced with Rashba semiconductors and suggests the possibility of manipulating the Gilbert damping by band engineering.

DOI: 10.1103/PhysRevLett.131.186703

As one of the key parameters in spin dynamics [1], Gilbert damping characterizes the rate of angular momentum transfer from spin to other degrees of freedom and determines the performance of a variety of spintronic devices, such as the magnetization switching time and the critical current density [2,3]. Manipulating the Gilbert damping of metallic ferromagnetic (FM) thin films or ferromagnet/nonmagnetic (NM) heterostructures remains one of the central interests in spintronics applications [1]. Both theoretical calculations and experimental works have demonstrated that the Gilbert damping can be controlled via modification of the strength of spin-orbit coupling ξ, the density of states at the Fermi energy $N(E_F)$, and the momentum scattering time τ of magnetic materials [4–8]. Apart from these factors, in heterostructures composed of ferromagnetic and nonmagnetic materials, magnetization dynamics in FM can transfer angular momentum and energy into NM in the form of electrons (or magnons) and phonons. The former mechanism is known as the spin-pumping effect [9–12], while the latter is termed the phonon pumping effect [13]. Both effects can lead to an enhanced damping in nonlocal form.

The on-demand control over the anisotropy of Gilbert damping is also crucial for both fundamental research and versatile spintronic device engineering and optimization. From the generalized Landau-Lifshitz-Gilbert equation, the Gilbert damping is a tensor rather than a scalar, implying that a rotational or orientational anisotropic phenomenon may be present [8,14–16]. However, experimental observations of the anisotropic Gilbert damping are rare due to the random scattering which occurs in both FM and NM layers. The orientational anisotropy of Gilbert damping has been observed only in the metallic ferromagnet/semiconductor interface of Fe/GaAs(001) and in epitaxial CoFe and CoFeB films [17–20]. On the other hand, Chen *et al.* recently predicted strong anisotropic damping due to the interfacial spin-orbit coupling in ultrathin magnetic films [21]. However, no obvious anisotropic damping was experimentally observed either in Pt/$Ni_{81}Fe_{19}$/Pt or in Pd/Fe [22,23]. Although several works on anisotropic damping have been reported, the possible mechanism of anisotropic damping is interpreted by either the anisotropic density of states, spin-orbit coupling, or momentum scattering time. Because damping from phonons is 6–30 times less than the intrinsic damping in magnetic films like Fe and Ni, excluding phonon contributions [24], to date, no direct relationship between band structures and Gilbert damping has been established. Therefore, a complete microscopic understanding of anisotropic damping, especially nonlocal Gilbert damping, is highly desirable.

Here, we reported the experimental observations of an anisotropic nonlocal Gilbert damping in Fe/α-GeTe bilayers via Ferromagnetic resonance (FMR) measurements. By comparing the angle-resolved photoemission

 © 2023 American Physical Society

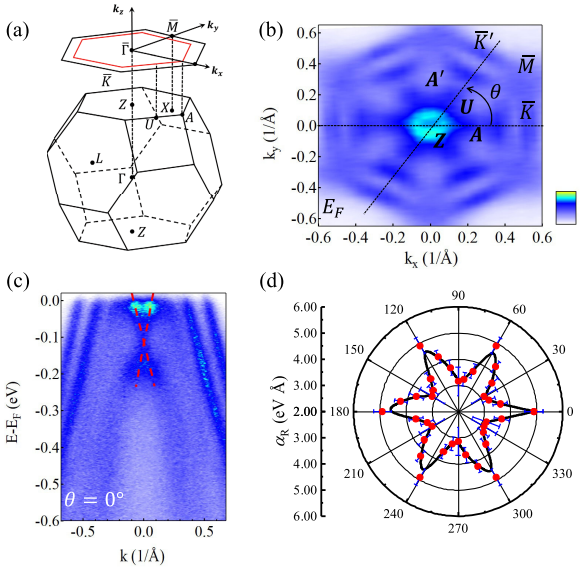

FIG. 1. Anisotropy of bulk Rashba bands. (a) 3D BZ of α-GeTe and its 2D BZ projected on the (0001) surface with high-symmetry points. (b) Fermi surface of α-GeTe(0001). The white dashed lines show the momentum position of the cuts. (c) Spectrum cut at $\theta = 0°$, the red dashed lines are the fitted lines for Rashba bands. The momentum cuts here are defined by the Fermi surface angle θ. (d) The anisotropic Rashba parameters α_R.

spectrum (ARPES) of GeTe (5 nm) with that of GeTe (30 nm), we confirm that the sixfold anisotropic damping of Fe/GeTe originates mainly from the sixfold symmetric band splitting of GeTe. Our findings suggest that the anisotropic damping can be realized by band engineering and an anisotropic spin-current injection in ferromagnet/α-GeTe heterostructures which opens a pathway toward adjusting anisotropic Gilbert damping in Rashba-based spintronic devices.

Figure 1(a) shows the bulk Brillouin zone of α-GeTe and its two-dimensional (2D) Brillouin zone projected on the (0001) surface with high symmetry points. The Fermi surface map is shown in Fig. 1(b), which presents two pockets around the Γ point. Previous studies [25,26] have identified these pockets as the anisotropic bulk Rashba spin-split bands. To understand the impact of the Dresselhaus effect on the bulk Rashba splitting, we cut the spectrum along different directions in k space as illustrated in Fig. 1(b). Figure 1(c) presents the momentum cut for $\theta = 0°$, where θ is defined by the Fermi surface angle (others shown in Supplemental Material [27], Fig. S4). It is evident that the size of bulk Rashba splitting first expands and then shrinks as the angle is increased. Especially, the smallest Rashba splitting is along $\bar{\Gamma} - \bar{M}$. The dispersion of Rashba bands is described by $E_{\pm} = (\hbar^2 \boldsymbol{k}^2 / 2m^*) \pm \alpha_R |\boldsymbol{k}|$. The Rashba parameter $\alpha_R \propto \xi E_Z$, where the ξ is the spin-orbit coupling strength of the materials and E_z is the electric field, which is perpendicular to the sample's surface. The peaks of the bulk Rashba bands are extracted by cutting the momentum distribution curves and fitting with a Lorentzian function. The red dashed lines in Fig. 1(c) are the best-fitted results. The in-plane angular dependence of Rashba parameters extracted from these fittings is shown in Fig. 1(d). One can observe from Fig. 1(d) that these Rashba parameters show a sixfold symmetry and the maximum $\alpha_R^{\max}$ and minimum $\alpha_R^{\min}$ are 4.89 eV Å and 3.15 eV Å, respectively.

To investigate the effect of anisotropic band splitting of GeTe on the magnetic damping of Fe/GeTe heterostructure, a 10 nm thick Fe layer was deposited on α-GeTe (shown in Supplemental Material [27]) [41]. Ferromagnetic resonance measurements (FMR) are carried out as illustrated in Fig. 2(a) where ϕ_H is the definition of magnetic field angle with respect to the GeTe$[11\bar{2}0]$. Figure 2(b) illustrates the dependence of FMR linewidth on resonance frequency (3.6 GHz–25 GHz) for the Fe(10 nm)/α-GeTe(30 nm) sample at $\phi_H = 0°$ and 30° (others shown in Supplemental Material [27], Fig. S8) and they can be fitted linearly with $R^2 \sim 0.99$. The fact that a linear frequency dependence of the linewidth persists throughout the frequency range provides convincing evidence that the extrinsic effects on the linewidths are not significant. In addition, by further taking the two-magnon scattering into account, we also fitted the experimental ΔH versus f using the equation $\Delta H_{\text{total}} = \Delta H_G + \Delta H_{2M} + \Delta H_0$ [42–44]. Here, $\Delta H_G = (4\pi\alpha f/\mu_0\gamma)$ represents the linewidth contribution from the Gilbert term;

$$\Delta H_{2M} = \Gamma \sin^{-1} \sqrt{\frac{\sqrt{(2\pi f)^2 + \left(\frac{2\pi f_0}{2}\right)^2} - \left(\frac{2\pi f_0}{2}\right)}{\sqrt{(2\pi f)^2 + \left(\frac{2\pi f_0}{2}\right)^2} + \left(\frac{2\pi f_0}{2}\right)}}$$

is the linewidth contribution from two-magnon scattering with $f_0 = (\gamma\mu_0/2\pi)M_{\text{eff}}$ and the strength of two-magnon scattering Γ. The ΔH_{total} (red solid lines), ΔH_G (blue solid lines), ΔH_{2M} (purple solid lines), and ΔH_0 (green solid lines) are shown in Fig. 2(d). We found that the maximum contribution of two-magnon scattering to the FMR linewidth is smaller than 10 Oe at 25 GHz at $\phi_H = 30°$, which is only 3% ($\Delta H_{2M}/\Delta H_{\text{total}}$) of the total FMR linewidth. These experimental results confirm that ΔH versus f is predominantly determined by the Gilbert contribution and the contribution of two-magnon scattering is negligible in our high-quality films. By excluding the contribution from extrinsic effects to the FMR linewidth (shown in Supplemental Material [27]), we obtain that the damping of Fe/GeTe at $\phi_H = 0°$ and 30° are 0.0113 ± 0.0001 and 0.0152 ± 0.0004, respectively.

Considering the phonon-related processes, the FMR mode can observably interact with the phonon when the modes' frequencies match, thereby resulting in an appreciable impact on the FMR linewidth. Nevertheless, in the case of GeTe, the frequency of its soft phonon modes

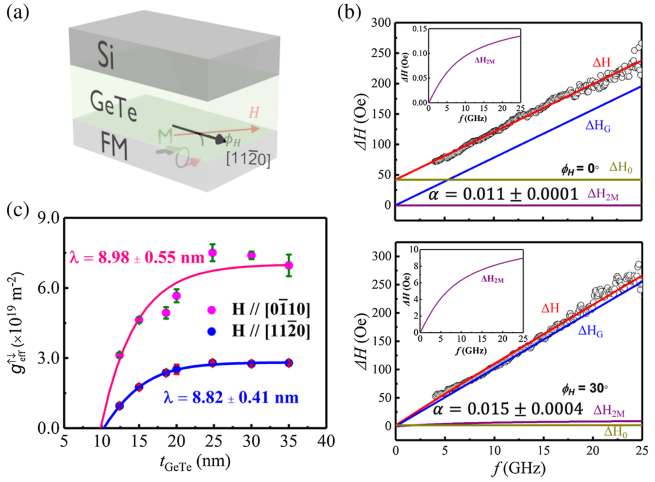

FIG. 2. FMR results of Fe/α-GeTe. (a) The FMR configuration in the ferromagnet/α-GeTe bilayer and the definition of the angles of external magnetic field ϕ_H with respect to the [11$\bar{2}$0] direction. (b) The relationship between resonant linewidth ΔH and resonant frequency f for $\phi_H = 0°$ and 30°. (c) SMC of Fe/α-GeTe bilayer as a function of the thickness of GeTe. The experimental data were measured at $H\|$GeTe[0$\bar{1}$10] and $H\|$GeTe[11$\bar{2}$0], respectively. The pink and blue lines are the fitted result using Eq. (1).

exceeds 2 THz at 300 K [45,46], while the magnitude of the spin current pumped into GeTe from the GeTe/Fe interface operates at the gigahertz scale. Besides that, the magnetization damping with a nonmonotonous dependence on FMR frequency [13,47]. In contrast, the damping enhancement from electronic spin pumping is independent of the FMR frequency. In our FMR measurements, we have observed that the resonant linewidth scales proportionally with the FMR frequency across all samples. This means the Fe/GeTe samples show a negligible phonon pumping contribution. According to previous studies [41,48], the spin-pumping effect exists in FM/GeTe bilayers. The difference in the damping may be caused by the spin-diffusion length along different crystal directions. We measured the spin-mixing conductances (SMC) $g^{\uparrow\downarrow}_{\text{eff}} = (4\pi M_s t_{\text{Fe}}/g\mu_B)(\alpha_{\text{eff}} - \alpha_0)$ (the efficiency of spin current injection from FM to GeTe) at two crystal directions $H\|$GeTe[0$\bar{1}$10] and $H\|$GeTe[11$\bar{2}$0] as shown in Fig. 2(c), respectively, and fit the data with the following equation [49],

$$g^{\uparrow\downarrow}_{\text{eff}} = g^{\uparrow\downarrow}\frac{1}{1+\left[2\sqrt{\frac{\varepsilon}{3}}\tanh\left(\frac{d_N}{\lambda_s}\right)\right]^{-1}}. \quad (1)$$

Here, M_s is the saturation magnetization, g is the Landé g factor, t_{Fe} is the thickness of the Fe layer, d_N and λ_s are the nonmagnetic layer thickness and spin-diffusion length of nonmagnetic layer, and ε is a dimensionless parameter proportional to the product of the atomic number and fine-structure constant in the nonmagnetic materials. The best-fitted results give that the spin diffusion length λ_s along two directions of [0$\bar{1}$10] and [11$\bar{2}$0] are (8.98 ± 0.55) nm and (8.82 ± 0.41) nm, and the effective SMC along GeTe[11$\bar{2}$0] are around $g^{\uparrow\downarrow}_{\text{eff}} \sim 6.97 \times 10^{19}$ m^{-2} and $g^{\uparrow\downarrow}_{\text{eff}} \sim 2.8 \times 10^{19}$ m^{-2}, respectively. In Fig. 2(c) a nearly 10 nm offset is shown in the fitting results, which arises from the thickness-dependent band structure of GeTe, in which the Rashba parameter was expressed by the scaling law discussed in our previous work [50]. As $d_N/\lambda_s \gg 1$, $\tanh(d_N/\lambda_s) = 1$. Therefore, the real part of the SMC, $g^{\uparrow\downarrow}$, can be calculated by measuring thicker Fe samples. The anisotropic damping $(\alpha_{[0\bar{1}10]} - \alpha_{[11\bar{2}0]})/\alpha_{[11\bar{2}0]})$ induced by the slight difference in spin diffusion length between these two directions is estimated to be smaller than 0.1%, suggesting that the anisotropic damping does not originate from the slight difference in spin diffusion length. These observations imply that the anisotropic nonlocal damping α_{sp} mainly originates from the anisotropy of $g^{\uparrow\downarrow}$, i.e., the anisotropic efficiency of spin current injection from Fe to GeTe.

Figure 3(a) shows the angular dependence of the effective damping of Fe(10 nm)/α-GeTe(30 nm) (blue

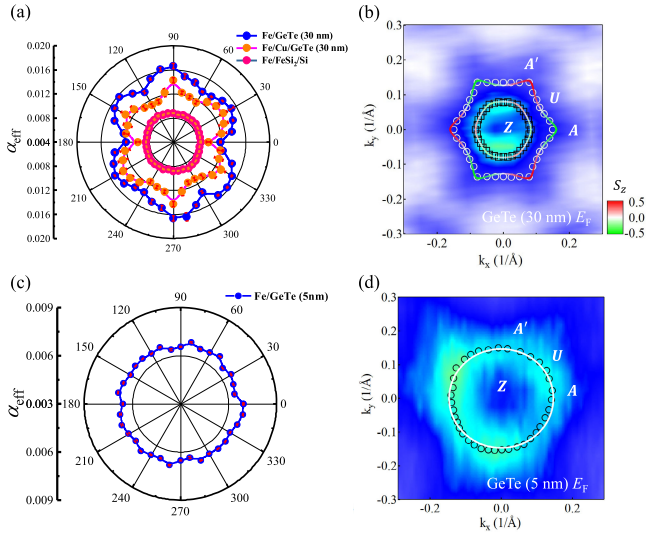

FIG. 3. Anisotropic damping of Fe/α-GeTe. (a) The angular dependence of the damping of Fe/α-GeTe(30 nm), Fe/Cu/α-GeTe, and reference sample Fe/FeSi$_2$/Si are shown by the blue, orange, and red circles, respectively. (b) The Fermi surface of bulk bands of 30 nm GeTe. The dark circles and green squares represent the peaks of the outer and inner spin-split bands, respectively. The solid lines are the fitted results with Eq. (2) and the color represents the z component of spin. The color bar is the magnitude of s_z. (c) The isotropic damping of Fe/α-GeTe(5 nm). (d) The Fermi surface of bulk bands of 5 nm GeTe. The black circles are the peaks of the bulk bands at the Fermi level. The solid line is the fitting result with Eq. (2) and the color [sharing the same color bar with (b)] represents the z component of spin.

dots), and the red dots show that of the reference sample $Fe/FeSi_2/Si$. The $FeSi_2$ buffer layer plays a significant role in the epitaxial growth of Fe(111) on Si(111) [51]. As a result, it has the same orientation as Fe deposited on α-GeTe. For 10 nm Fe deposited on α-GeTe, the Gilbert damping shows a clear sixfold symmetry. However, this phenomenon is not observed in the Fe reference sample. To rule out the possible proximity effect, a 3.0 nm Cu spacer layer is inserted between Fe and GeTe [52]. The damping of the Fe/Cu(3 nm)/GeTe trilayer sample is still sixfold symmetric, which demonstrates that the anisotropic damping does not arise from a magnetic proximity effect. We can clearly find that the damping of Fe/Cu/GeTe is higher than the reference sample $Fe/FeSi_2/Si$ [Fig. 3(a)], due to the spin-pumping effect. The increase in damping for Fe/GeTe as compared to the Fe/Cu/GeTe originates from the magnetic proximity effect between Fe and GeTe. Therefore, we can conclude that the anisotropic damping is due to the spin-pumping effect.

We further analyzed the band dispersions at the Fermi surface of α-GeTe. Because of the anisotropic Rashba parameters in α-GeTe [Fig. 1(d)], the spin splitting comes from the coexistence of the Rashba and cubic Dresselhaus effects [26,53]. This anisotropic band splitting can be described by the following dispersion [26,54],

$$E_{\pm}(k) = E_0(k) \pm \sqrt{\alpha_R^2 k^2 + \eta^2 k^6 \cos^2(3\theta)}. \qquad (2)$$

Here, $E_0(k) = \hbar^2 k^2/2m^*$ and η represents the strength of the cubic Dresselhaus effect. Figure 3(b) shows the Fermi surface of bulk states of α-GeTe. The momentum position on the Fermi surface of the outer and inner anisotropic spin split bands are represented by the dark circles and the green squares, respectively, all of which are extracted from momentum distribution curves. The solid lines are the fitted results by Eq. (2). The best-fitted results give the strength of cubic Dresselhaus effect $\eta \sim 100$ eV Å^3. Because of the cubic Dresselhaus effect which couples to σ_Z, the spin polarization of the bulk states should have an out-of-plane spin component s_Z, which can be calculated through $s_z = \cos(3\theta)/\sqrt{\cos^2(3\theta) + [1/(ka)^4]}$ [41], where $a \equiv \sqrt{\eta/\alpha_R}$. As shown in Fig. 3(b), the magnitude of s_Z of the outer bands is anisotropic with a sixfold symmetry and has a maximum of around 0.41 along $Z - A$. According to our previous work [37], the bulk band structures of GeTe are modified due to the polarization varied with thickness. Therefore, we found the damping and the bulk band structures of a control sample of Fe/GeTe (5 nm) are isotropic as shown in Figs. 3(c) and 3(d). We use Eq. (2) to fit the band structure of 5 nm GeTe and the Dresselhaus effect $\eta \sim 1$ eV Å^3. The maximum s_z is around 0.003 along with $Z - A$ as shown in Fig. 3(d). Therefore, the s_z component of spin polarization is likely a major influence on the anisotropic damping.

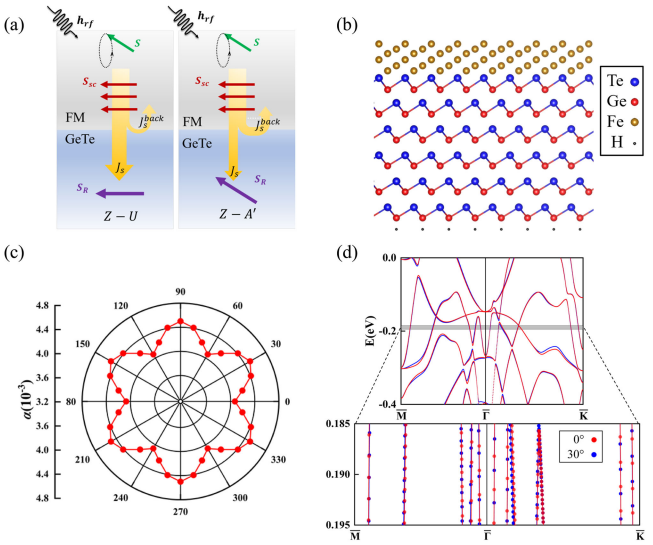

FIG. 4. The spin pumping model and DFT calculated anisotropy of Gilbert damping in Fe/α-GeTe bilayer. (a) The schematic of spin current injection from the FM layer to the GeTe layer. The left and right are taken at U and A' point of GeTe, respectively. (b) Schematic illustration of Fe/α-GeTe crystal structure. (c) The angular dependence of the DFT-calculated Gilbert damping parameter is shown by the red circles. (d) The DFT-calculated band structure of Fe/α-GeTe at $\phi_H = 0°$ (red lines and dots) and $\phi_H = 30°$ (blue lines and dots). The bottom panel shows a close-up of the bands in the energy window from −0.195 to −0.185 eV.

As shown in Fig. 4(a), along $Z - U$, where $s_Z = 0$, the strength of the cubic Dresselhaus effect can be neglected. Hence, the possibility of the scattering between the spin of α-GeTe bulk states and spin current in this direction is lower than that in the direction of $Z - A'$, which has a nonzero s_Z. As a result, the isotropic spin current source generated in the FM experiences an anisotropic spin potential due to the s_Z of the bulk states of α-GeTe and thereby enables the anisotropic SMC.

Considering the spin current with in-plane spin polarization from the FM injected into α-GeTe, the spin scattering can occur at both the α-GeTe surface states and the bulk states. To obtain a deeper understanding of the contribution of the surface states of α-GeTe to the anisotropic damping, we use density functional theory (DFT) calculations to estimate this contribution [Fig. 4(b) shows the crystal structure in our DFT calculations]. On the basis of the modulated Fermi level by Ge vacancies, we set the Fermi level at −0.19 eV to obtain the Gilbert damping parameter in the Fe/α-GeTe heterostructure. Figure 4(c) shows the DFT-calculated Gilbert damping parameter α^{DFT} of Fe/α-GeTe with an Fe layer magnetized in plane. We can see that the angular dependence of α_{DFT} has a sixfold symmetry, and the minimum and maximum damping occurs at $H\|[11\bar{2}0]$ and $H\|[0\bar{1}10]$, respectively. As shown in Fig. 4(d), DFT-calculated band structures at $H\|[11\bar{2}0]$

and $H\|[0\bar{1}10]$ are visibly different. Such differences in band structures naturally give rise to different Gilbert damping parameters. However, by analyzing the Gilbert damping calculated by DFT, we obtain the following results: (i) the DFT calculated Gilbert damping parameters are smaller than the experimentally measured ones; (ii) the experimentally measured anisotropy ratio $(\alpha_{[0\bar{1}10]} - \alpha_{[11\bar{2}0]})/\alpha_{[11\bar{2}0]} \sim 36.3\%$ is obviously larger than that obtained by DFT $\left(\alpha^{DFT}_{[0\bar{1}10]} - \alpha^{DFT}_{[11\bar{2}0]}\right)/\alpha^{DFT}_{[11\bar{2}0]} \sim 11\%$. These discrepancies between the experimentally measured and DFT-calculated magnetic damping originate from the contribution of damping from spin pumping, which is not included in our DFT calculations. Another likely reason is that the effect of interface coupling becomes weaker as the thickness of the Fe film is increased. In conclusion, both the bulk and surface states of α-GeTe can contribute to an anisotropic damping factor, but the main contribution to the anisotropic damping is the bulk band.

Finally, the top Fe layer is replaced by permalloy (Py), which has a much weaker magnetic anisotropy, and the same experiments were repeated. The results show that the damping of Py/α-GeTe/Si also possesses a pronounced sixfold symmetry while the reference sample Py/Si exhibits an isotropic damping (shown in Supplemental Material [27]). Therefore, we can conclude that the anisotropic damping originates from the anisotropic spin-pumping effect caused by the anisotropic bulk band splitting of GeTe.

A previous study reported an anisotropic damping in a spin valve structure $Co_{50}Fe_{50}/Cr/Ni_{81}Fe_{19}$ [55]. In this Letter, spin pumping in the polycrystalline $Ni_{81}Fe_{19}$ generates a spin current anisotropically absorbed by the crystalline $Co_{50}Fe_{50}$ due to spin torque, thus resulting in an anisotropic damping of $Ni_{81}Fe_{19}$. In this case, the underlying mechanism for the anisotropic damping does not involve the direction dependence of the band structure and spin-orbit coupling. In contrast, this Letter shows for the first time that the symmetry of the anisotropic magnetic damping can be influenced by the symmetry of band structures in an adjacent material and address the origin of spin pumping related to the spin polarization of Fermi surface.

In summary, we provide direct experimental evidence for the anisotropic nonlocal Gilbert damping in Fe/α-GeTe (30 nm) bilayers. Compared with the isotropic damping sample in Fe/GeTe (5 nm) bilayers, this anisotropic damping is mainly caused by the anisotropic band splitting of bulk states of α-GeTe. The experimental realization of an anisotropic nonlocal Gilbert damping by band engineering provides new opportunities for control over the damping and developing new applications in spintronics devices, such as the anisotropic spin-flip efficiency in spin-transfer torque-based devices.

This work was supported by the National Key R&D Program of China (Grant No. 2022YFA1403302) and the National Natural Sciences Foundation of China (Grants No. 52031015, No. U22A20115, and No. 12104518), GBABRF-2022A1515012643 and GBABRF-202201011118. DFT calculations are performed on Tianhe-II.

*Corresponding author: li.yan@kaust.edu.sa
†Corresponding author: houysh@mail.sysu.edu.cn
‡Corresponding author: zhcheng@iphy.ac.cn

[1] I. Zutic, J. Fabian, and S. Das Sarma, Spintronics: Fundamentals and applications, Rev. Mod. Phys. **76**, 323 (2004).
[2] R. Kikuchi, On the minimum of magnetization reversal time, J. Appl. Phys. **27**, 1352 (1956).
[3] K. Lee and S. H. Kang, Development of embedded STT-MRAM for mobile system-on-chips, IEEE Trans. Magn. **47**, 131 (2011).
[4] I. Garate and A. MacDonald, Gilbert damping in conducting ferromagnets. II. Model tests of the torque-correlation formula, Phys. Rev. B **79**, 064404 (2009).
[5] S. Mizukami *et al.*, Long-lived ultrafast spin precession in manganese alloys films with a large perpendicular magnetic anisotropy, Phys. Rev. Lett. **106**, 117201 (2011).
[6] G. Woltersdorf, M. Kiessling, G. Meyer, J. U. Thiele, and C. H. Back, Damping by slow relaxing rare earth impurities in $Ni_{80}Fe_{20}$, Phys. Rev. Lett. **102**, 257602 (2009).
[7] M. A. W. Schoen, D. Thonig, M. L. Schneider, T. J. Silva, H. T. Nembach, O. Eriksson, O. Karis, and J. M. Shaw, Ultra-low magnetic damping of a metallic ferromagnet, Nat. Phys. **12**, 839 (2016).
[8] K. Gilmore, M. D. Stiles, J. Seib, D. Steiauf, and M. Fahnle, Anisotropic damping of the magnetization dynamics in Ni, Co, and Fe, Phys. Rev. B **81**, 174414 (2010).
[9] Y. Tserkovnyak, A. Brataas, and G. E. Bauer, Enhanced Gilbert damping in thin ferromagnetic films, Phys. Rev. Lett. **88**, 117601 (2002).
[10] Y. T. Fanchiang, K. H. M. Chen, C. C. Tseng, C. C. Chen, C. K. Cheng, S. R. Yang, C. N. Wu, S. F. Lee, M. Hong, and J. Kwo, Strongly exchange-coupled and surface-state-modulated magnetization dynamics in Bi_2Se_3/yttrium iron garnet heterostructures, Nat. Commun. **9**, 223 (2018).
[11] T. Chi *et al.*, Dirac-surface-state modulated spin dynamics in a ferrimagnetic insulator at room temperature, Sci. Adv. **4**, eaas8660 (2018).
[12] J. C. Rojas-Sanchez *et al.*, Spin to charge conversion at room temperature by spin pumping into a new type of topological insulator: Alpha-Sn films, Phys. Rev. Lett. **116**, 096602 (2016).
[13] S. Streib, H. Keshtgar, and G. E. W. Bauer, Damping of magnetization dynamics by phonon pumping, Phys. Rev. Lett. **121**, 027202 (2018).
[14] M. Fahnle, D. Steiauf, and J. Seib, The Gilbert equation revisited: Anisotropic and nonlocal damping of magnetization dynamics, J. Phys. D Appl. Phys. **41**, 164014 (2008).
[15] V. L. Safonov, Tensor form of magnetization damping, J. Appl. Phys. **91**, 8653 (2002).
[16] J. Seib, D. Steiauf, and M. Fahnle, Linewidth of ferromagnetic resonance for systems with anisotropic damping, Phys. Rev. B **79**, 092418 (2009).

[17] L. Chen *et al.*, Emergence of anisotropic Gilbert damping in ultrathin Fe layers on GaAs(001), Nat. Phys. **14**, 490 (2018).

[18] Y. Li *et al.*, Giant anisotropy of Gilbert damping in epitaxial CoFe films, Phys. Rev. Lett. **122**, 117203 (2019).

[19] L. Chen, S. Mankovsky, M. Kronseder, D. Schuh, M. Prager, D. Bougeard, H. Ebert, D. Weiss, and C. H. Back, Interfacial tuning of anisotropic Gilbert damping, Phys. Rev. Lett. **130**, 046704 (2023).

[20] H. Xu, H. Chen, F. Zeng, J. Xu, X. Shen, and Y. Wu, Giant anisotropic Gilbert damping in single-crystal Co-Fe-B(001) Films, Phys. Rev. Appl. **19**, 024030 (2023).

[21] K. Chen and S. Zhang, Spin pumping in the presence of spin-orbit coupling, Phys. Rev. Lett. **114**, 126602 (2015).

[22] W. Cao, L. Yang, S. Auffret, and W. E. Bailey, Nearly isotropic spin-pumping related Gilbert damping in $Pt/Ni_{81}Fe_{19}/Pt$, Phys. Rev. B **99**, 094406 (2019).

[23] Y. Li *et al.*, Isotropic non-local Gilbert damping driven by spin pumping in epitaxial Pd/Fe films on MgO(001) substrates, New J. Phys. **21**, 103040 (2019).

[24] J. A. C. Bland and B. Heinrich, *Ultrathin Magnetic Structures III: Fundamentals of Nanomagnetism* (Springer, New York, 2005).

[25] M. Liebmann *et al.*, Giant Rashba-type spin splitting in ferroelectric GeTe(111), Adv. Mater. **28**, 560 (2016).

[26] D. Di Sante, P. Barone, R. Bertacco, and S. Picozzi, Electric control of the Giant Rashba effect in bulk GeTe, Adv. Mater. **25**, 509 (2013).

[27] See Supplemental Material at http://link.aps.org/supplemental/10.1103/PhysRevLett.131.186703 for methods, additional data, and discussions, which includes Refs. [28–40].

[28] R. Wang, J. E. Boschker, E. Bruyer, D. D. Sante, S. Picozzi, K. Perumal, A. Giussani, H. Riechert, and R. Calarco, Toward truly single crystalline GeTe films: The relevance of the substrate surface, J. Phys. Chem. C **118**, 29724 (2014).

[29] G. Kresse and J. r. Hafner, *Ab initio* molecular dynamics for liquid metals, Phys. Rev. B **47**, 558 (1993).

[30] G. Kresse and J. r. Furthmüller, Efficient iterative schemes for *ab initio* total-energy calculations using a plane-wave basis set, Phys. Rev. B **54**, 11169 (1996).

[31] J. P. Perdew, K. Burke, and M. Ernzerhof, Generalized gradient approximation made simple, Phys. Rev. Lett. **77**, 3865 (1996).

[32] P. E. Bl chl, Projector augmented-wave method, Phys. Rev. B **50**, 17953 (1994).

[33] G. Kresse and D. Joubert, From ultrasoft pseudopotentials to the projector augmented-wave method, Phys. Rev. B **59**, 1758 (1999).

[34] S. Grimme, J. Antony, S. Ehrlich, and H. Krieg, A consistent and accurate *ab initio* parametrization of density functional dispersion correction (DFT-D) for the 94 elements H-Pu, J. Chem. Phys. **132**, 154104 (2010).

[35] Y. S. Hou and R. Q. Wu, Strongly enhanced Gilbert damping in 3*d* transition-metal ferromagnet monolayers in contact with the topological insulator Bi_2Se_3, Phys. Rev. Appl. **11**, 054032 (2019).

[36] G. Liang, L. Cheng, J. Zha, H. Cao, J. Zhang, Q. Liu, M. Bao, J. Liu, and X. Zhai, *In-situ* quantification of the surface roughness for facile fabrications of atomically smooth thin films, Nano Res. **15**, 1654 (2021).

[37] S. S. Kalarickal, P. Krivosik, M. Wu, C. E. Patton, M. L. Schneider, P. Kabos, T. J. Silva, and J. P. Nibarger, Ferromagnetic resonance linewidth in metallic thin films: Comparison of measurement methods, J. Appl. Phys. **99**, 093909 (2006).

[38] Y. B. Xu, D. J. Freeland, M. Tselepi, and J. A. C. Bland, Anisotropic lattice relaxation and uniaxial magnetic anisotropy in $Fe/InAs(100)\text{-}4\times2$, Phys. Rev. B **62**, 1167 (2000).

[39] Y. Li *et al.*, Drag effect induced large anisotropic damping behavior in magnetic thin films with strong magnetic anisotropy, J. Phys. Condens. Matter **33**, 175801 (2021).

[40] A. Conca, S. Keller, M. R. Schweizer, E. T. Papaioannou, and B. Hillebrands, Separation of the two-magnon scattering contribution to damping for the determination of the spin mixing conductance, Phys. Rev. B **98**, 214439 (2018).

[41] C. Rinaldi *et al.*, Evidence for spin to charge conversion in GeTe(111), APL Mater. **4**, 032501 (2016).

[42] R. Arias and D. L. Mills, Extrinsic contributions to the ferromagnetic resonance response of ultrathin films, Phys. Rev. B **60**, 7395 (1999).

[43] K. Lenz, H. Wende, W. Kuch, K. Baberschke, K. Nagy, and A. Janossy, Two-magnon scattering and viscous Gilbert damping in ultrathin ferromagnets, Phys. Rev. B **73**, 144424 (2006).

[44] R. Arias and D. L. Mills, Extrinsic contributions to the ferromagnetic resonance response of ultrathin films, J. Appl. Phys. **87**, 5455 (2000).

[45] C. Wang, J. Wu, Z. Zeng, J. Embs, Y. Pei, J. Ma, and Y. Chen, Soft-mode dynamics in the ferroelectric phase transition of GeTe, npj Comput. Mater. **7**, 118 (2021).

[46] G. Kremer *et al.*, Field-induced ultrafast modulation of Rashba coupling at room temperature in ferroelectric α-GeTe(111), Nat. Commun. **13**, 6396 (2022).

[47] R. Schlitz, L. Siegl, T. Sato, W. Yu, G. E. W. Bauer, H. Huebl, and S. T. B. Goennenwein, Magnetization dynamics affected by phonon pumping, Phys. Rev. B **106**, 014407 (2022).

[48] S. Varotto *et al.*, Room-temperature ferroelectric switching of spin-to-charge conversion in germanium telluride, Nat. Electron. **4**, 740 (2021).

[49] H. Nakayama, K. Ando, K. Harii, T. Yoshino, R. Takahashi, Y. Kajiwara, K. Uchida, Y. Fujikawa, and E. Saitoh, Geometry dependence on inverse spin Hall effect induced by spin pumping in $Ni_{81}Fe_{19}/Pt$ films, Phys. Rev. B **85**, 144408 (2012).

[50] X. Yang *et al.*, Three-dimensional limit of bulk Rashba effect in ferroelectric semiconductor GeTe, Nano Lett. **21**, 77 (2021).

[51] J. Ye, W. He, Q. Wu, H. L. Liu, X. Q. Zhang, Z. Y. Chen, and Z. H. Cheng, Determination of magnetic anisotropy constants in Fe ultrathin film on vicinal Si(111) by anisotropic magnetoresistance, Sci. Rep. Uk **3**, 2148 (2013).

[52] X. Fan, J. Wu, Y. P. Chen, M. J. Jerry, H. W. Zhang, and J. Q. Xiao, Observation of the nonlocal spin-orbital effective field, Nat. Commun. **4**, 1799 (2013).

[53] R. Fei, S. Yu, Y. Lu, L. Zhu, and L. Yang, Switchable Enhanced Spin Photocurrent in Rashba and Cubic Dresselhaus Ferroelectric Semiconductors, Nano Lett. **21**, 2265 (2021).

[54] L. Fu, Hexagonal warping effects in the surface states of the topological insulator Bi_2Te_3, Phys. Rev. Lett. **103**, 266801 (2009).

[55] A. A. Baker, A. I. Figueroa, C. J. Love, S. A. Cavill, T. Hesjedal, and G. van der Laan, Anisotropic absorption of pure spin currents, Phys. Rev. Lett. **116**, 047201 (2016).